

Seismic responses of a large underground structure in liquefied soils by FEM numerical modelling

Haiyang Zhuang^{1,2} · Zhonghua Hu¹ ·
Xuejian Wang¹ · Guoxing Chen¹

Received: 13 February 2015 / Accepted: 13 June 2015 / Published online: 1 July 2015
© Springer Science+Business Media Dordrecht 2015

Abstract A large underground subway structure could be severely damaged in a strong earthquake, such as the seismic damages of Daikai subway station in the 1995 Kobe earthquake. After the 1995 Kobe earthquake, the effects of earthquakes on underground structure became a hot topic. According to the seismic damage characteristics of the pipelines buried in the liquefiable soils, a large underground structure may be damaged ever more severely by the liquefaction. To examine the dynamic properties of saturated liquefiable soil, an existed constitutive model is revised and implanted into the commercial FEM software. Then the nonlinear seismic responses of large underground subway structures built in liquefiable soils are analyzed by a numerical modeling. The results of the comprehensive numerical analysis indicate that the existing subway station has a significant effect on the liquefaction of the nearby soils that are likely to be liquefied. The around sand soils under the suggested depth 20 m may be also liquefied under the influence of the large subway station, which should be non-liquefiable sand in many related codes of China. The subway station floats up as soon as the nearby soils are liquefied, and the soils accordingly flow from the lateral foundation to the bottom foundation of the subway station. It is also found that the floating of the subway station is completely out of sync in the main vibration stage of the inputted ground motions and the rising stage of the pore pressure, and it also lags behind in the main vibration stage for a considerable time and begins to stabilize only when the vibration weakens sharply and is close to zero. Generally, the dynamic softening soils under the subway station also have great effect on the seismic response of the large subway station.

Keywords Sand liquefaction · Underground subway station · Seismic response · FEM method · Soil-structure interaction

✉ Haiyang Zhuang
Zhuang7802@163.com

¹ Institute of Geotechnical Engineering, Nanjing Tech University, Nanjing 210009, China

² School of Civil Engineering, Shandong University, Jinan 250061, China

1 Introduction

Structures have been severely damaged by sand liquefaction in earthquakes, such as 1964 Niigata Earthquake in Japan, 1971 San Fernando Earthquake in the United States, and 1995 Kobe Earthquake in Japan. Large liquefaction-induced deformation is one of the major damages. The geological conditions of a large underground subway structure are very complicated and can change dramatically. Sand liquefaction can obviously affect the seismic behaviors of a large underground subway structure.

The seismic responses of underground structures have received increasing attention since 1995 Kobe Earthquake in Japan, during which many underground subway structures were damaged and some were completely destroyed. The damage of the Dakai subway station has been studied in detail through numerical modeling and shaking table tests (Iwatate et al. 2000; Hashash et al. 2001; Zhuang et al. 2008a, b). As for the sand liquefaction effect, some researches have investigated the seismic behaviors of the tunnels that are built in liquefiable soils (Chou et al. 2001; Azadi and Hosseini 2010; Unutmaz 2014). In addition, numerical modeling and model tests have also been performed to study the seismic behaviors and responses of the subway stations built in liquefiable soils (Liu and Song 2006; Chen et al. 2013, 2015; Chou et al. 2010; Chian and Madabhushi 2012; Chian et al. 2014).

To investigate the seismic behaviors and responses of a large underground subway station with three spans and two floors which is built in liquefiable soil, an efficient numerical method should be developed to evaluate the large liquefaction-induced deformation of the ground around the underground structure. This paper addresses the deficiency of a commercial FEM software in modeling the dynamic properties of liquefiable soil by developing a constitutive model and inputting it into Abaqus software (Abaqus 6.10-1). To simulate the liquefied-induced large deformation of the ground, an arbitrary Lagrangian–Eulerian (ALE) adaptive meshing method is used to maintain a high-quality mesh system for the soil throughout the analysis process when large deformations or losses of soil occur, allowing the mesh to move independently. Finally, an advanced numerical model is constructed to model the nonlinear static and dynamic coupling interactions between the liquefiable ground and the underground structure. Comparison is made between the results and the existing studies. The conclusions presented in this work are expected to provide an efficient numerical method for simulating large liquefied-induced deformations and present important insights to the soil liquefaction effects on the seismic behaviors and responses of a large underground structure.

2 Case study

To date, in Nanjing, China, four subway lines are under operation and three new lines are under construction. The Yangzi River runs through Nanjing city. Large amounts of sands have been carried downstream near Nanjing year after year and a very thick and loose sand layer has been deposited in the area. The natural soil stratum condition of the ground near the Yangzi River is shown in Table 1 according to the indoor tests and some site tests. The grain size distribution curve of the sand in the area is shown in Fig. 1. Here the shear modulus of the fine-silty sand layer changes from 39.3 to 118 MPa with its buried depth. At present, the subway station model with two layers and three spans is widely used in China. Accordingly, a typical subway station in Nanjing is selected as the research object,

Table 1 Properties of soils surrounding the underground structure

Soil profiles	Thickness (m)	G_0 (MPa)	Unit weight (kN/m ³)	φ (°)	Elastic modulus (MPa)	Poisson's ratio ν	Porosity n
Mucky soil	2.0	25.2	19.0	16	1.0	0.45	-
Mucky silty clay	2.0	30.3	17.8	16	1.0	0.45	-
Fine-Silty Sand (moderate solid)	46.1	39.3 -118	19.0	35	7.5	0.422	0.474
Clay (hard)	10.0	476.0	19.3	21	3.2	0.42	-

and its cross-sectional dimensions and distributed rebar are shown in Fig. 2. The longitudinal distance of the columns is 9.12 m.

3 Numerical model

3.1 Station and soil model

A 2-D nonlinear static and dynamic coupling model is developed for the soil-underground structure dynamic interaction. In this numerical model, four-node plane strain-reduced integration elements are used to mesh the soil foundation and the subway station structure; 2-D beam elements are embedded into the concrete to model the rebar in it. Based on Liao’s study (2013), the maximal height of element h_{max} of the shear motion propagating in the soil should be determined by

$$h_{max} = \left(\frac{1}{75} - \frac{1}{160} \right) V_s / f_{max} \tag{1}$$

where V_s is the shear and compression motion velocity, which can be deduced by $G_0 = \rho V_s^2$, and ρ is the density of the soil. f_{max} is the maximal vibration frequency of the inputted motion. Accordingly, the maximal element height of the soil from the top to the bottom of the ground ranges from 1 to 3 m.

The dynamic boundary condition of the soil foundation must be addressed with effective methods. At present, two methods can be used to model the static and dynamic coupling boundary conditions: one is the artificial transmitting boundary and the other is the artificial constrained boundary. To simplify the calculation process, the latter one is used to deal with the lateral boundary of ground. According to this method, the lateral boundary is constrained in the horizontal direction, and the horizontal reaction forces (RF) at the nodes on the lateral boundary are output at the end of the static analysis. Prior to the dynamic analysis, the lateral boundary condition is released in the horizontal direction with a horizontal RF that is reserved by the artificial loading method and constrained in the vertical direction. The boundary condition changing process is shown in Fig. 3. To weaken the reflected wave effect on the lateral boundary of ground, the horizontal distance from the lateral boundary to the underground structure is set as 90 m, and the damping factor of the elements near the boundary are amplified fivefold.

The standard calculated module of Abaqus 6.10-1 software is used to analyze this dynamic problem. The ALE adaptive meshing method is used to maintain a high-qualified meshing system for the soil foundation during the entire process, allowing the meshes to move independently from the material when the large deformation of liquefied soils occurs. The finite element meshes of the soil-structured interaction system are shown in Fig. 4.

The whole subway station is meshed by using four-node plane strain elements except for the rebar is meshed by the two-node beam elements. The rebar is implanted into the concrete and the sliding between the concrete and the steel can be neglected. The meshing plan for the subway station is shown in Fig. 5.

A dynamic contact mechanical model and its equilibrium equations can be established and solved by using different dynamic contact algorithms such as *Lagrangian Multiplier Method* and *Penalty Function Method* to model the dynamic contact between the soil and the underground structure. This simulation method practically simulates dynamic contacts with large displacement sliding and separating on the interfaces between two different materials.

In the normal direction of the interface, the normal contact compressive stress mutually transfers via the contact constraint. The element nodes on the surfaces satisfy *Hooke's Law* and the *Harmonized Condition of Displacement*. If the master surface is separated from the slaver surface, the contact constraint will be cancelled and the contact boundary condition on the interface will be transferred to the common free boundary.

The Tangential Contact Shear Stress (TCSS) is also transferred in the tangential direction of the interface. If the value of the TCSS is larger than the critical value of the shear stress τ_{crit} , slipping will occur on the interface. Coulomb's Friction Law is used to simulate the tangential mechanics behaviors and can be expressed as

$$\tau_{crit} = \mu \cdot P \quad (2)$$

where μ is the friction coefficient of the interface between the soil and the concrete (0.4 in this paper) and P is the normal contact stress on the interface.

3.2 Constitutive model for concrete

The concrete damaged-plasticity constitutive model presented by Jeeho and Fenves (1998) models the material mechanical behavior of concrete. The strength level of concrete used in this underground structure is No. C30, and its material properties are shown in Table 2. As we know, it is difficult to directly model the crack damage of concrete by using the

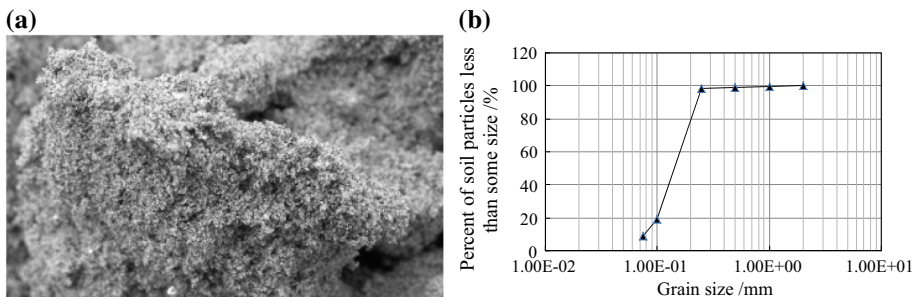


Fig. 1 Grain size distribution curve of the sand. **a** The sand, **b** grain size distribution curve

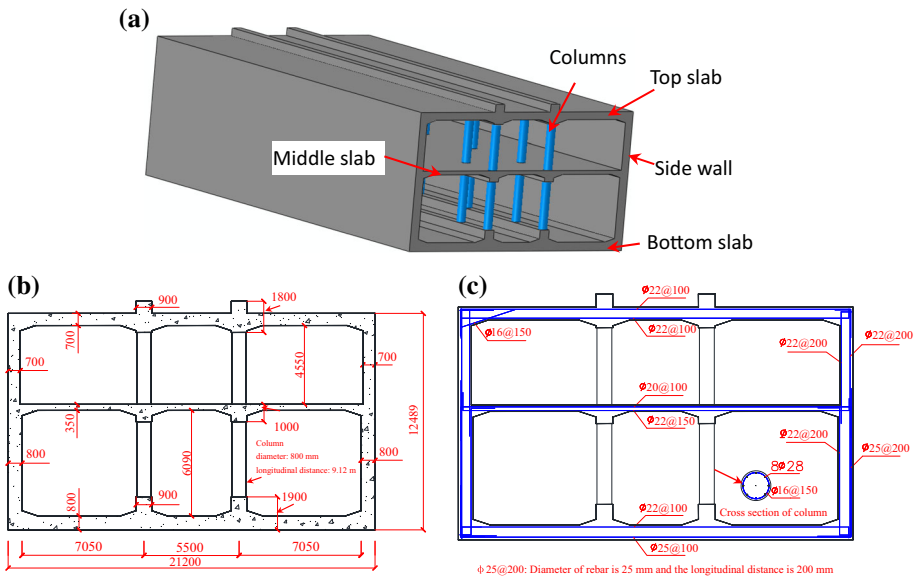


Fig. 2 The cross-sectional dimensions and distributed rebar of the subway station. **a** The 3-D model of subway station, **b** cross-sectional dimensions, **c** distributed rebar designed

FEM method. To simulate the post-failure behavior of concrete, a simplified method is given by Jeeho et al. based on a fracture energy-cracking criterion to specify a stress-displacement curve instead of a stress-strain curve as shown in Tables 3 and 4.

However, when a 2-D model is used to simulate the subway station, two rows of middle columns must be equivalent to two walls along the long axial direction of the subway station. According to the principle of equivalent stiffness, the equivalent walls should have the same lateral deformation stiffness of the original columns. Accordingly, the equivalent elastic modulus of the concrete for the walls can be deduced by

$$E_{eq}I_{eq} = E_cI_c/D \tag{3}$$

where $E_{eq}I_{eq}$ is the equivalent stiffness of the unit width wall in long axial direction of the subway station, E_cI_c is the stiffness of a column, and D is the column space in long axial direction of the subway station. Accordingly, the equivalent elastic modulus of the concrete for the middle columns is about 3.85×10^3 MPa, and the equivalent elastic modulus of the reinforcing steel is about 1.2×10^6 MPa in the 2-D beam sections.

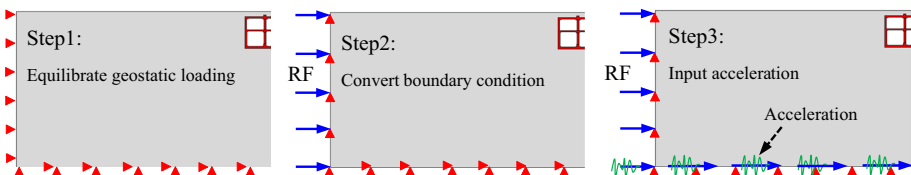


Fig. 3 Boundary conditions changing process in analysis

The damping property of concrete in this work is a 3 % approximate fraction of critical damping for the first mode of vibration of the underground structure. Assuming Rayleigh stiffness proportional damping, the factor β required to provide a fraction ξ_1 of critical damping for the first mode is given as

$$\beta = 2\xi_1/\omega_1 \tag{4}$$

where $\xi_1 = 3\%$. Based on a natural frequency extraction analysis of the interaction system, the first Eigen frequency is $\omega_1 = 0.45$ rad/s. Accordingly, β is designated as 0.133 s.

3.3 Constitutive model for the soils

Yang (2000) presented a constitutive model to simulate the dynamic properties of the liquefiable sands with a yield function as

$$f = \frac{3}{2}(s - p_a\alpha) : (s - p_a\alpha) - M^2 p_a^2 = 0 \tag{5}$$

$$s = \sigma - p\delta, \quad p_a = p - a, \quad p = \frac{1}{3}tr(\sigma), \quad a = c/\tan\varphi \tag{6}$$

where s is the deviatoric stress tensor, σ is the effective Cauchy stress tensor, δ is the Kronecker delta, p is the effective mean normal stress, a is a material constant, c and φ are the cohesion and friction angle of the soil. α is the kinematic deviatoric tensor defining the coordinates of the yield surface center in the deviatoric stress subspace, and M is a material parameter related to the friction angle φ .

In this model, the hardening parameters M and α determine the dimension and location of the subsequent active yield surface. With continuous loading, the yield surface becomes larger and moves continuously. Therefore, the increment of these two hardening parameters must be correctly calculated to determine the shape of the subsequent yield surface. These two hardening parameters are calculated by an interpolation method in the original model developed by Yang et al., and the shear modulus does not change when the yield surface locates between the two fixed yield surfaces which are determined by equally dividing the stress space within the damage yield surface of soil. Specifically, a quadratic equation must be solved to determine the value of the hardening parameter M for each increment.

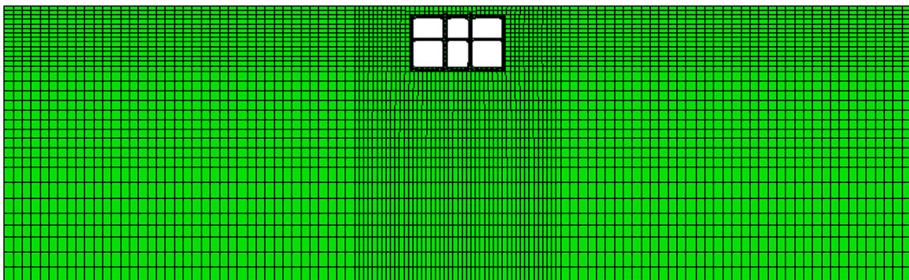


Fig. 4 Finite element meshing system for the soil-structure interaction system

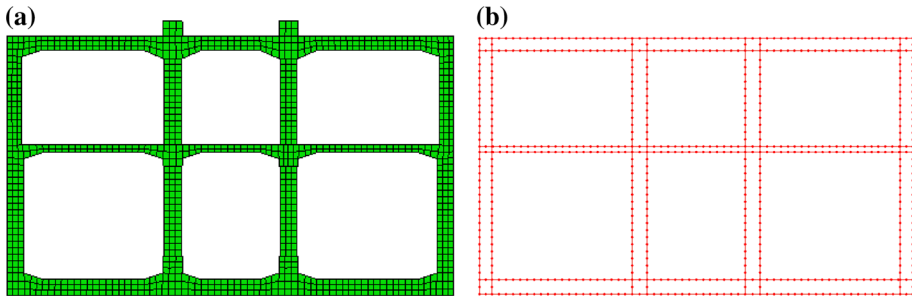


Fig. 5 Meshing plan for the subway station. **a** Subway station meshed by solid elements, **b** rebar meshed by beam elements

Table 2 Material properties of the concrete No. C30

Parameters	Value	Parameters	Value
Elastic modulus	$E_0 = 3.0 \times 10^4$ MPa	Limited compressive yield stress	$\sigma_{cu} = 20.1$ MPa
Poisson's ratio	$\nu = 0.18$	Initial tensile yield stress	$\sigma_{t0} = 2.4$ MPa
Density	$\rho = 2450$ kg/m ³	Compression stiffness recovery parameter	$\omega_c = 1.0$
Dilation angle	$\psi = 36.31^\circ$	Tensile stiffness recovery parameter	$\omega_t = 0.0$
Initial compressive yield stress	$\sigma_{c0} = 13$ MPa	Damage variables	d_c, d_t (Tables 4, 5)

To make the yield surface and the shear modulus change sequentially after each increment, a widely available hardening rule (Zhuang and Chen 2006) is introduced to replace that of this model. The multi-yield surface concept is thus adopted to allow all yield surfaces to be translated in stress space by the stress point without change in form. They consecutively touch and push each other but cannot intersect. Therefore, when the loading reverses, the prior yield surface is defined as the reversed yield surface f_r . In the subsequent loading process, all active yield surfaces f_i are then tangent with the reversed yield surface at the reversed stress point, and their centers in the deviatoric stress subspace change along the direction θ defined from the center of the reversed yield surface to the reversed stress point, as shown in Fig. 6. Accordingly, the increment of model hardening parameters M and α of the active yield surface is given as

$$dM^{t+\Delta t} = - \frac{3(s - p_a\alpha) : ds + \sqrt{6}M \cdot dp \cdot (s - p_a\alpha) : \theta + 2J' \cdot M \cdot dp}{\sqrt{6}M \cdot p_a \cdot (s - p_a\alpha) : \theta + 2J' \cdot p_a} \Big|_t \quad (7)$$

$$d\alpha^{t+\Delta t} = - \sqrt{\frac{2}{3}} (M^t \cdot dp + p_a \cdot dM^{t+\Delta t}) : \theta - dp \cdot \alpha^t \quad (8)$$

where

$$J' = \sqrt{\frac{3}{2} (s - p_a\alpha) : (s - p_a\alpha)} \quad (9)$$

Table 3 Relationship of the compression stress and damage factor versus plastic strain

Plastic strain (%)	0.0	0.04	0.08	0.12	0.16	0.20	0.24	0.36	0.50	0.75	1.00
Compressive stress (MPa)	14.64	17.33	19.44	20.10	20.18	18.72	17.25	12.86	8.66	6.25	3.98
d_c	0.0	0.113	0.246	0.341	0.427	0.501	0.566	0.714	0.824	0.922	0.969

Table 4 Relationship of the tensile stress and damage factor versus cracking displacement

Cracking displacement (mm)	0.0	0.066	0.123	0.173	0.220	0.308	0.351	0.394	0.438	0.482
Tensile stress (MPa)	2.4	1.617	1.084	0.726	0.487	0.219	0.147	0.098	0.066	0.042
d_t	0.0	0.381	0.617	0.763	0.853	0.944	0.965	0.978	0.987	0.992

Table 5 Material parameters for Nanjing sand

Parameters	Value	Parameters	Value
Reference shear modulus	$G_0 = 33$ MPa	Contraction parameters	$c_1 = 0.12, c_2 = 0$
Reference mean pressure	$p_0 = 100$ kPa	Hardening parameters	$e_1 = 0.8, e_2 = 2.8$
Pressure dependence exponent	$n_p = 0.5$	Dilation parameters	$d_1 = 0.5, d_2 = 0$
Friction angle	$\phi = 31.6^\circ$	Locking strain parameters	$y_1 = 0.015, y_2 = 0$
Phase transformation angle	$\phi_{pt} = 26.5^\circ$	Locking release pressure	$p_y = 0.5$ kPa
Residual strength pressure	$a = 5$ kPa	Slip strain parameter	$y_{sl} = 0.01$

Based on the study by Pyke (1979), the elastoplastic tangent modulus H under cyclic loading is given as

$$H = 2G \left(1 - \frac{r}{r_{\max}} \right)^2 \tag{10}$$

where G is the initial shear modulus, which can be determined by

$$G = G_0 \left(\frac{p_a}{p_0 - a} \right)^n \tag{11}$$

where G_0 is the moduli measured at the reference confine pressure p_0 , n is a material parameter defined from a laboratory test (in this paper, $p_0 = 100$ kPa, $n = 0.5$), r is the radius of the active yield surface in the deviatoric stress plane, and r_{\max} is the radius of the corresponding damage surface in the deviatoric stress plane. Therefore, Eq. (10) can be rewritten as

$$H = 2G \left(1 - \frac{M}{M_{\max}} \right)^2 \tag{12}$$

where M_{\max} is the model parameter for the damaged surface F that corresponds to the active yield surface. Similar to the Drucker–Prager model (Drucker and Prager 1952), M_{\max} can be defined as

$$M_{\max} = \frac{6 \sin \varphi}{3 - \sin \varphi} \tag{13}$$

The plastic modulus H' can then be expressed as

$$H' = \left(\frac{1}{H} - \frac{1}{2G_0} \right)^{-1} \tag{14}$$

Other parameters associated with the proposed model that can be identified by the expressions are shown in the reference Yang (2000). Moreover, this model has been convincingly verified against a wide range of relevant experiments (Yang et al. 2003).

In this paper, the above model is compiled by the Fortran computer language and implanted into the Abaqus software. A 3-D numerical model is then developed to model the dynamic responses of a sand sample tested in a dynamic triaxial machine with the confining stress (σ_c) being 100 kPa and the magnitude of cyclic loading (F_d) being 288 N (Zhuang and Chen 2011; Zhuang et al. 2012). The predicted axial-strain time histories and the strain–stress curve by the developed model are compared with the test results of the soil sample, as shown in Fig. 7, which shows that the compiled subroutine is available. According to the tests by a GDS Instrument Company triaxial machine, the material parameters for the Nanjing sand are shown in Table 5.

The non-liquefiable soils are simulated by a visco-plastic model developed by Zhuang and Chen (2006). It can model the dynamic accumulation deformation and the hysteretic graph of soils under the irregular cyclic loadings. Meanwhile, this model has also been verified by some experiments and compared with other models by Zhuang and Chen (2006), which proved that it can predict well the stress–strain curves of the soft soils and is well used to predict the nonlinear seismic responses of the free field, as shown in Fig. 8.

As far as the nonlinear earthquake response of site is concerted, the hysteresis damping of soil has been considered in dynamic elasto-plastic models. The additional viscous damping of soil should be considered separately. According to the Rayleigh damping, the matrix of viscous damping is calculated as:

$$[C] = \alpha_0[M] + \alpha_1[K] \tag{15}$$

In this paper, the damping matrix is supposed to be calculated by stiffness matrix $[K]$ only. Accordingly, the parameters α_0 and α_1 can be calculated as:

$$\alpha_0 = 0, \quad \alpha_1 = 2\zeta_1/\omega_1 \tag{16}$$

where the parameter ζ_1 is the damping ratio of the fundamental mode and its value is

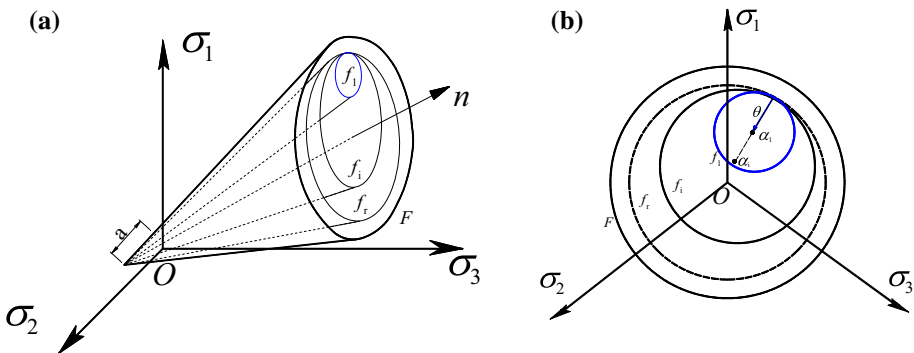


Fig. 6 Yield surface in principal stress space and deviatoric plane. **a** Effective principal stress space, **b** deviatoric plane

between 2 and 5 %. The parameter ω_1 is the natural vibration frequency of the dynamic interaction system.

3.4 Input motions

Prior to the dynamic simulation of the earthquake, the interaction system is subjected to gravity loading and hydrostatic pressure. In the Abaqus/Standard analysis, these loads are specified in two consecutive static steps. The Kobe earthquake motion (Kobe motion), the El-Centro earthquake motion (El-Centro motion) and the Nanjing artificial earthquake motion (Nanjing motion) are selected as the input ground motions from the bedrock in the horizontal direction. The KB motion was recorded during the Kobe earthquake in 1995. It is a representative near-field earthquake motion with an epicentral distance being 0.4 km; the main frequency range of the vibration is from 0.5 to 4 Hz, the strong motion duration is 4.5–12 s. After 20 s, and the acceleration amplitude is very small and is approximately zero. The EI motion was recorded in the Imperial Valley earthquake in 1940, with an original peak ground acceleration (PGA) of 0.349 g. The duration of the strong earthquake was approximately 26 s. The NJ motion was calculated by the COMPSYN software developed by the IEM of the China Earthquake Administration. Its original peak acceleration was 0.15 g, and the duration of a strong earthquake was approximately 22 s. To model different earthquake intensities, the PGA of the original earthquake motions is adjusted to 0.1, 0.2, and 0.3 g, respectively. The three earthquake motions are shown in Fig. 9, and their curves for the dynamic coefficient defined as the normalized acceleration response are shown in Fig. 10.

4 Seismic response of the interaction system

4.1 Liquefaction of ground

To demonstrate the efficiency of the developed constitutive model, the shear stress–strain curve of a liquefied soil element near the underground structure is shown in Fig. 11. The dilation of the saturated sand during the loading phase is obvious. In the loading cycle during liquefaction, it can be observed that a large change in shear strain from a contractive to a dilative response occurs with minimal change in shear stress in the vicinity of phase transformation.

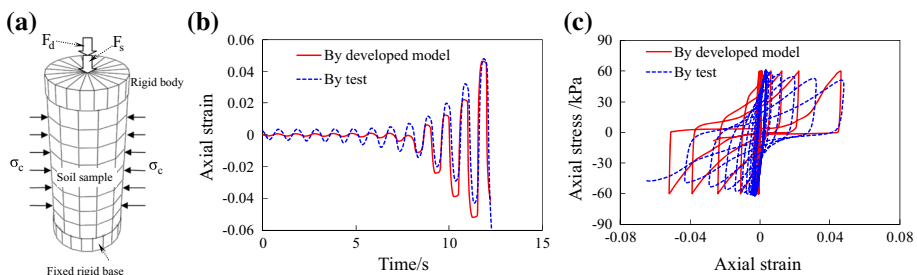


Fig. 7 Predicted results of the FEM method compared with the test results. **a** Soil sample model, **b** axial-strain time histories, **c** strain–stress curve

The dynamic pore pressure ratio is used to judge the liquefaction state of the ground. The results of Kobe motion are shown in Fig. 12. In this figure, SDV52 denotes the dynamic pore pressure ratio. When the input PGA of KB motion is 0.1 g, the entire ground surrounding the subway station does not liquefy except for a very small area near the subway station, as shown in Fig. 12a. However, the ground near the subway station is obviously liquefied with an input PGA of 0.2 g, as shown in Fig. 12b. When the input PGA increases to 0.3 g, the liquefaction extends dramatically in the horizontal direction, as shown in Fig. 12c. The soils far away from the subway station in the horizontal direction are either liquefied or very near to the liquefied state obviously. At the same time, the liquefaction area extends dramatically in depth with the input PGA increasing from 0.1 to 0.3 g. It is apparent that the existing subway station has an obvious effect on the liquefaction potential of the surrounding saturated soils which are liquefied more easily than soils that are far away from the subway station.

Figure 13 shows the contour diagrams of the dynamic pore pressure ratio for the three selected earthquake motions with the input PGA = 0.3 g. It shows that the frequency content of the input motion has a weak effect on the liquefied area around the subway station. However, during the different input motions, the excess pore water pressure response of the ground under the subway station changes obviously, which should be affected by the uplifting of the subway station and the input motions together. Generally, the liquefied area is the largest with input PGA = 0.2 g for KB motion and is the smallest for NJ motion. As a new finding, it also shows that the existing subway station makes the surrounding liquefied area enlarge in vertical space. The maximal depth of the liquefied area around the subway station is approximately 24 m, which is larger than the suggested depth of 20 m under which the soils should be decided to be non-liquefiable soils in many related codes of China. This new finding should be considered in the seismic liquefaction estimation of the ground for a large underground structure.

To further show the effect of the subway station on the liquefaction state of the ground, Fig. 14 shows the dynamic pore pressure responses of the ground at the same level as that of the middle slab with a input PGA = 0.2 g. In Fig. 14, the dynamic pore pressure response of the ground becomes stronger with its horizontal distance to the subway station becoming greater. However, the dynamic pore pressure ratio near the subway station is at the maximum, which proves that the soils close to the subway station are more apt to be liquefied even though the corresponding pore pressure response is lower than other places with the same depth. This finding also shows that a floating subway station should have a significant effect on the dynamic pore pressure response of the ground close to it, which

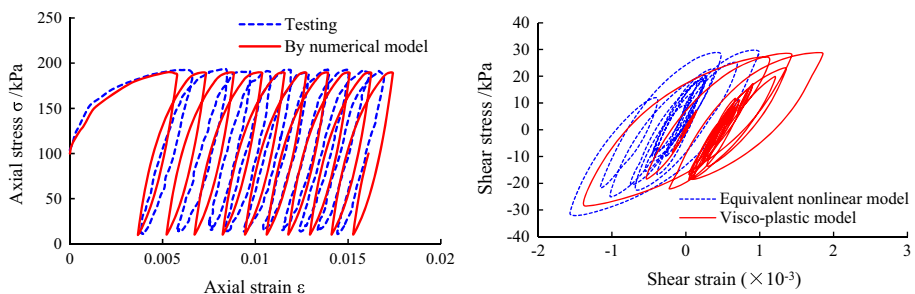


Fig. 8 Predicted stress–strain curves compared with the test result and that by another model

also agrees with the findings by the shaking table tests for the seismic response of a large underground structure buried in a liquefiable foundation (Chen et al. 2007).

To show the effect of the input earthquake motions, Fig. 15 shows the curves of the dynamic pore pressure ratio when the different earthquake motions are input respectively. Generally, it shows that the rapidly rising stage of pore pressure is closely related to the beginning of the strong vibration in each earthquake motion, and then the pore pressure keeps in a stable state after the strong vibration.

4.2 Liquefaction-induced deformation

When the soils surrounding the subway station are liquefied, the subway station obviously floats upward. Figure 16 shows the displacement vector of the ground surrounding the subway station when the input PGA is 0.2 g. The figure shows that the lateral liquefied soils surrounding the subway station flow to the bottom, which further aggravates the uplift of the subway station. This finding may better explain the working mechanism of a cutoff wall in reducing the uplift induced by soil liquefaction of a large underground structure, which has also been studied by Liu and Song (2006) by a numerical modelling. That is to say, the cutoff wall under the subway station can block the liquefied soils flowing from the lateral ground to the bottom of the subway station. Furthermore, for a small pipe buried in liquefiable soils, the flowing manner of the liquefied soils around the pipe is also discovered by Chian et al. (2014). Namely, the shape and dimension of the underground structure should have little effect on the flowing manner of liquefied soils around it.

To evaluate the effect on the dynamic deformation of the ground surface of the subway station, the final settlement curves of the ground surface are shown in Fig. 17 when the KB motion is input. This figure shows that the differential settlement is particularly obvious on the ground surface within 10 m to the subway station, which should have a significant effect on the foundation stability of the nearby aboveground buildings and the buried pipes. In addition, when the input PGA increases from 0.2 to 0.3 g, the settlement caused by the earthquake subsidence quickly increases accordingly.

Based on Figs. 15 and 16, it can be found that the earthquake-induced settlement differences at the ground surface near the subway station are primarily caused by the floating of subway station. The significant settlement at the ground surface 10–30 m far from the subway station is affected by the lateral liquefied soils flowing to the bottom of the subway station. The settlement of the ground surface far away from the subway station should be primarily caused by earthquake subsidence.

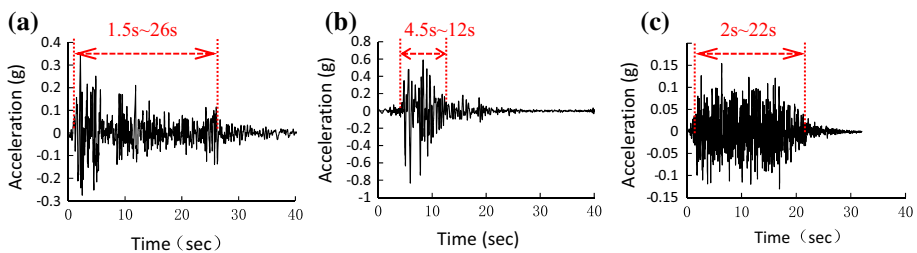


Fig. 9 Original time-histories of the acceleration used as the input motion. **a** El-Centro motion, **b** Kobe motion, **c** Nanjing motion

Fig. 10 Curves of dynamic coefficient for different earthquake motions

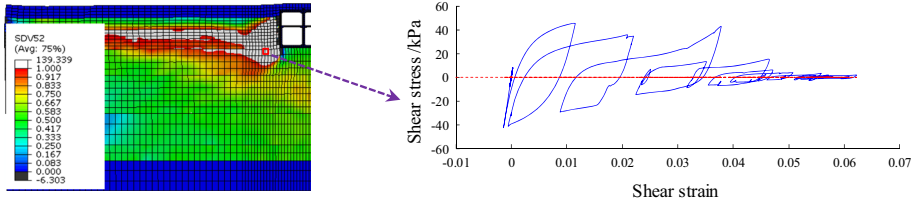
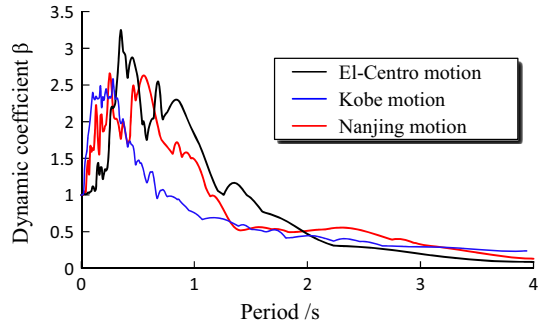


Fig. 11 Shear stress–strain curve of a liquefied soil element in the Kobe motion

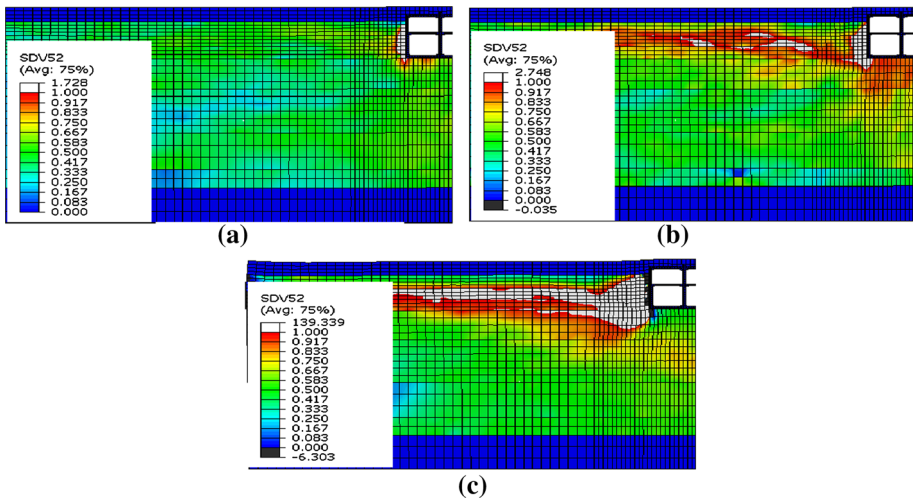


Fig. 12 Distributed contour diagram of the dynamic pore pressure ratio in Kobe motion. **a** PGA = 0.1 g, **b** PGA = 0.2 g, **c** PGA = 0.3 g

Figure 18 shows the settlement curves of the ground surface when the input PGA is 0.3 g for different earthquake motions. It shows that an earthquake motion has little effect on the underground structure floating. However, it has greater effect on the settlement of the ground surface far away from the subway station. Generally, the duration of the strong

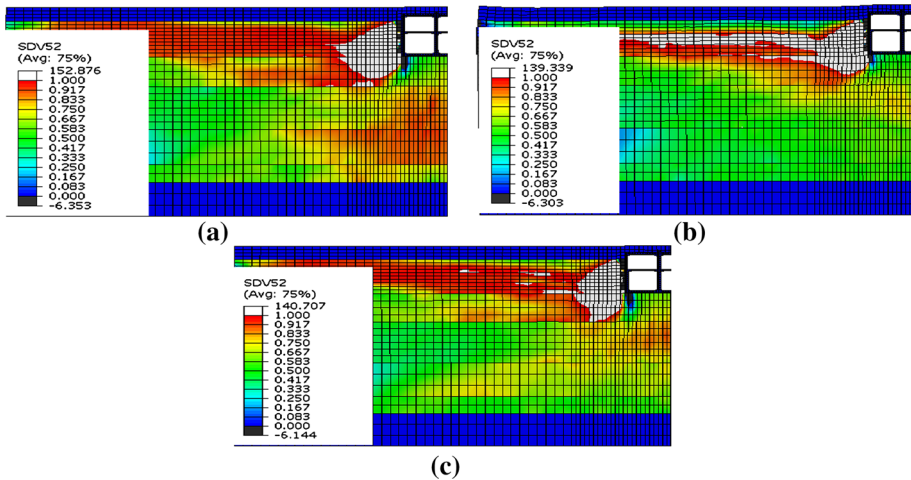


Fig. 13 Distributed contour diagram of the dynamic pore pressure ratio with PGA = 0.2 g in the different earthquakes. **a** EI-Centro motion, **b** Kobe motion, **c** Nanjing motion

vibration for each earthquake motion should be the main factor to aggravate the vertical settlement of the ground surface.

During an earthquake, the subway station may float upward and a seismic subsidence may occur. Figure 19 shows the seismic vertical displacement time history of the subway station and the point where the ground surface had its maximum settlement. In Fig. 19a, the floating of the subway station clearly increases when the input PGA increases from 0.1 to 0.2 g, which is primarily aggravated by the rising pore pressure and the liquefaction of the soils surrounding the subway station. In particular, the subway station floats by approximately 25 cm when the input PGA increases to 0.3 g.

In addition, as the input PGA increases, the floating of the subway station begins earlier and ends later. The main floating stage of the subway station is approximately 6–20 s with different input PGA for Kobe motion which obviously lags behind the main rising stage of the pore pressure. After 20 s, when the acceleration amplitude approaches zero, the earthquake-induced floating of the subway station nearly stops. Based on the above analysis, the floating of the subway station is also completely out of sync with the main

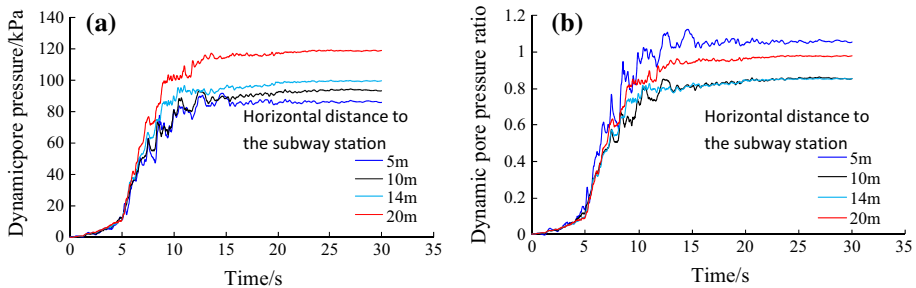


Fig. 14 Dynamic pore pressure responses at the lateral ground of the subway station with PGA = 0.2 g in Kobe motion

vibration stages of the input ground motion, and will stop only when the vibration nearly ceases. This phenomenon has also been found from a pipe buried in liquefiable soils according to the numerical modelling and the model test by Chian et al. (2014).

In Fig. 19b, it can be found that the seismic vertical displacement on the ground surface steadily increases. The main seismic settlement stage is approximately 5–20 s. After 20 s, the seismic vertical displacement increases slowly, mainly due to the dissipation of the seismic pore pressure.

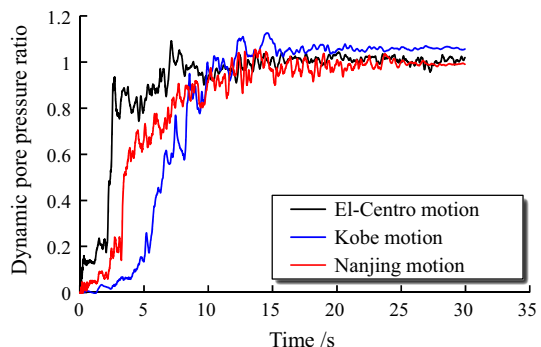
In general, when the lateral ground is nearly non-liquefied in the Kobe motion with the input $PGA = 0.1$ g, the floating of the subway station and the seismic settlement of the ground surface are all very slight. When the lateral ground is partially liquefied with the input $PGA = 0.2$ g, the subway station floats with a slight increase. However, when the lateral ground is substantially liquefied with the input $PGA = 0.3$ g, the subway station floats severely, with a maximal differential settlement between the ground surface over the subway station and the lateral ground surface of approximately 50 cm. For another two earthquake motions, the above changing rules are also found true.

According to the study by Iida et al. (1996), the Dakai subway station was likely damaged by a destructive horizontal force caused by the relative displacement between the base level and the ceiling level due to subsoil movement. Although this type of movement may have a minor effect on a small underground structure, the effect can be significant on a larger underground structure such as a subway station.

Figure 20 shows the relative displacement responses between the base level and ceiling level of the subway station. In Fig. 20, the maximum amplitudes of the relative displacement responses also increase with the increasing input PGA . However, the relative displacement responses are weakened after the soils surrounding the subway station are liquefied. In particular, at an input PGA of 0.2 g, a large horizontal residual deformation of the subway station is evident at the end of the earthquake. However, when the input PGA is 0.1 or 0.3 g, this type of residual deformation significantly weakened.

When another two motions are input respectively, the above changing rules for the residual deformation are muted, as shown in Fig. 21. When the input PGA increases from 0.2 to 0.3 g for the El-Centro motion, the horizontal residual deformation of the subway station becomes larger. However, the changes are very trivial based on the Nanjing motion input. By analyzing Figs. 21 and 22, it is proved that the isolation degree of the softening soil under the subway station should be the main factor for the different changing tendencies of the horizontal residual deformation of the subway station. That is to say, it

Fig. 15 Dynamic pore pressure responses at the lateral ground for the different earthquake motions



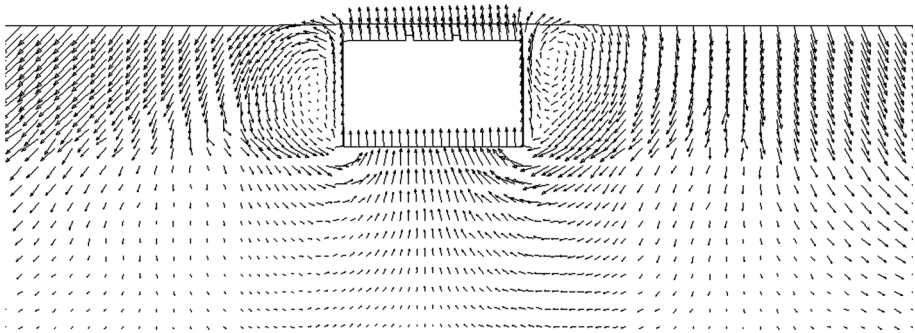


Fig. 16 Displacement vectors around the subway station with $PGA = 0.2\text{ g}$ in Kobe motion

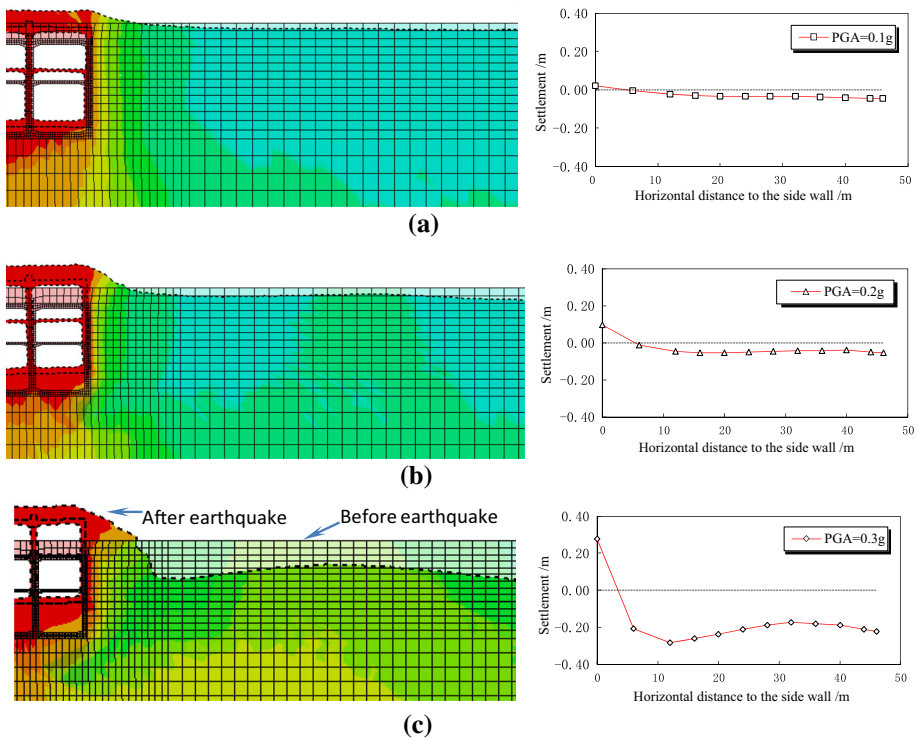


Fig. 17 Settlement curves of the ground surface in Kobe ground motion (in scale: 20). **a** $PGA = 0.1\text{ g}$, **b** $PGA = 0.2\text{ g}$, **c** $PGA = 0.3\text{ g}$

should be affected by the soil yielding response and the liquefaction state of the around ground, and the input motion characteristics should also affected it.

Based on the suggested elastic interlayer displacement angle for the frame-shear wall reinforced concrete structure in the Chinese Code of Aseismic Design of Buildings (Code No. GB50011-2010), the relative displacement between the base level and the ceiling level of the subway station should be 1.56 cm, corresponding to the elastic interlayer

Fig. 18 Settlement curves of the ground surface with $PGA = 0.3\text{ g}$ for the deferent earthquake motions

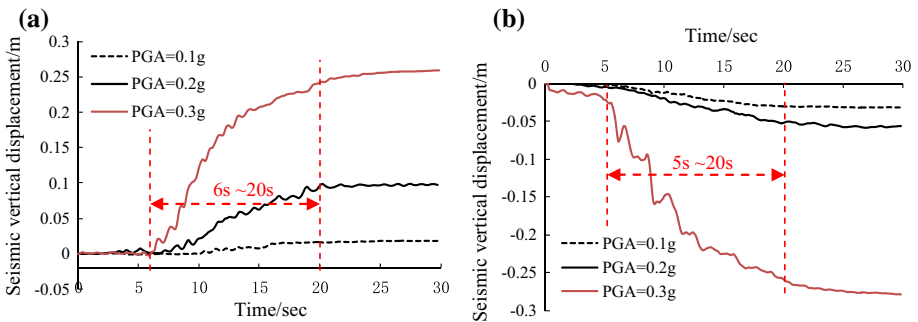
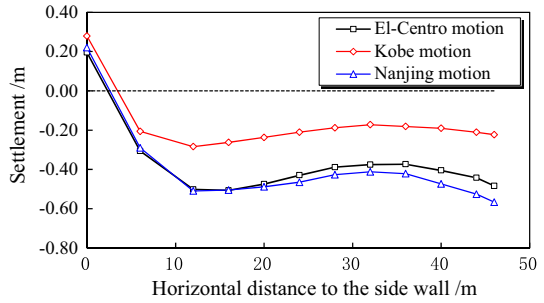


Fig. 19 Seismic vertical displacement time histories of the subway station and ground surface in Kobe motion. **a** Subway station floating, **b** seismic settlement of ground surface

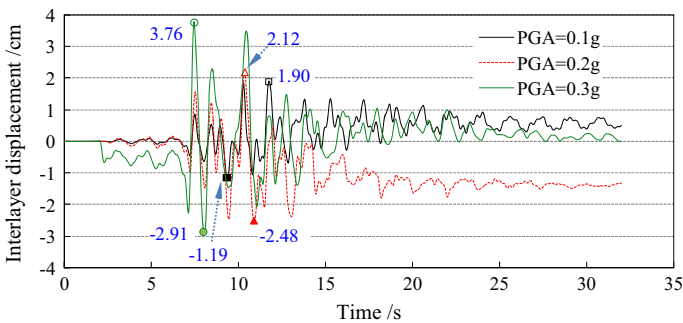


Fig. 20 Horizontal relative displacement responses of the subway station in Kobe motion

displacement, proving that the subway station should respond in the plastic state when the input PGA is 0.1 g for the maximal relative displacement is approximately 1.9 cm . When the input $PGAs$ increase to 0.2 and 0.3 g , the remaining relative displacements at the end of the earthquake increase to 2.48 and 3.76 cm , respectively. In general, the maximal relative displacement of the subway station increases monotonously with increasing PGA input.

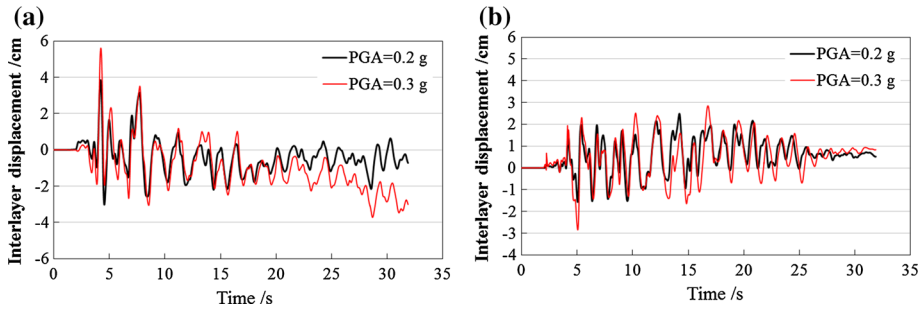


Fig. 21 Horizontal relative displacement responses of the subway station in the different motions. **a** El-Centro motion, **b** Nanjing motion

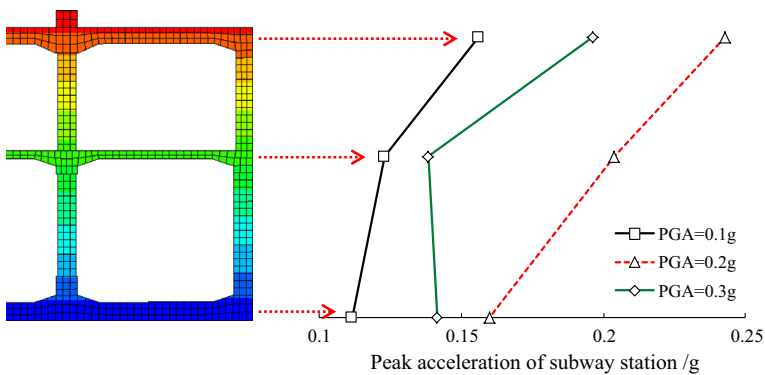
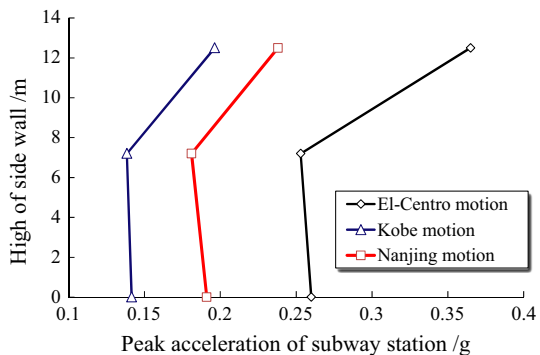


Fig. 22 Acceleration responses for the slabs of the subway station in Kobe motion

Fig. 23 Acceleration responses at the slabs of the subway station with PGA = 0.3 g in the different motions



4.3 Acceleration response of subway station

Figure 22 shows the PGA of response acceleration at the subway station slabs. When the input PGA increases from 0.1 to 0.2 g, the PGA of response acceleration also increases at each slab of the subway station. The PGAs of the acceleration responses also increase

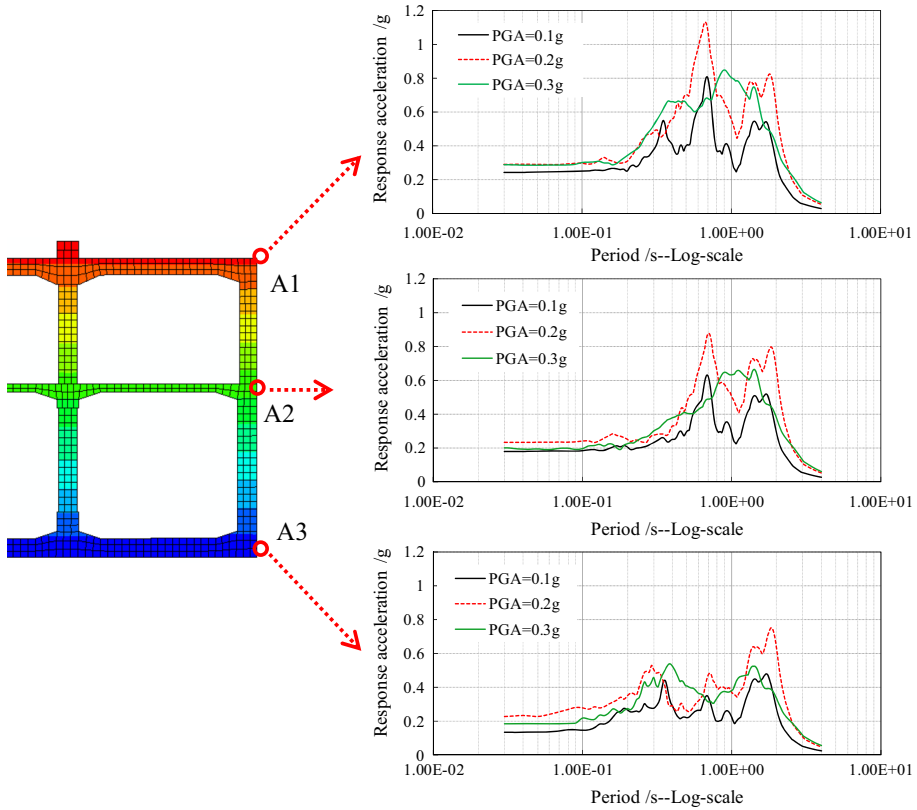


Fig. 24 Elastic response acceleration spectra of the subway station in Kobe motion

along the height of the subway station. However, when the input PGA increases from 0.2 to 0.3 g, the PGA of response acceleration notably decreases and the PGA no longer increases along the height of the subway station. These changes should be affected by the dynamic strength softening of the soils under the subway station and the liquefied degree of the lateral ground, which has also been observed in the past earthquakes (Trifunac 2003).

To show the effect of the input earthquake motions, Fig. 23 shows the PGA of response acceleration at the slabs of the subway station with input PGA = 0.3 g. As a result, the PGA of response acceleration at the middle slab of the subway station is smaller than that of the bottom slab, and then it increases obviously at the top slab. This finding is obviously inconsistent with the acceleration response rule for the general ground structure, and the soil-underground structure interaction should be the main factor. In addition, the PGAs of response acceleration are the smallest with input PGA = 0.3 g for the Kobe motion and they are the largest for the El-Centro motion due to the different isolation degrees of the softening soils under the subway station for different input earthquake motions.

Figure 24 shows the elastic response spectra of the accelerations at the slabs of the subway station with a damping ratio of 5 %. Generally, the response accelerations are magnified in a wide period from 0.2 to 3.0 s with the input PGA of 0.1 g. However, when the input PGA increases to 0.2 g, the period when the response accelerations are magnified narrows to be 0.4–2 s. Additionally, the response accelerations are magnified mainly at

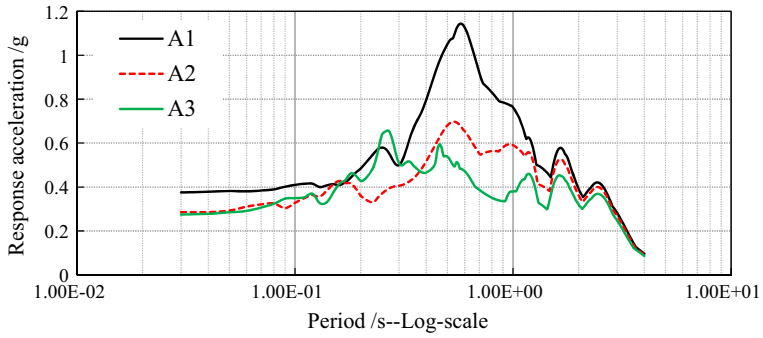


Fig. 25 Elastic response acceleration spectra of the subway station with PGA = 0.3 g in El-Centro motion

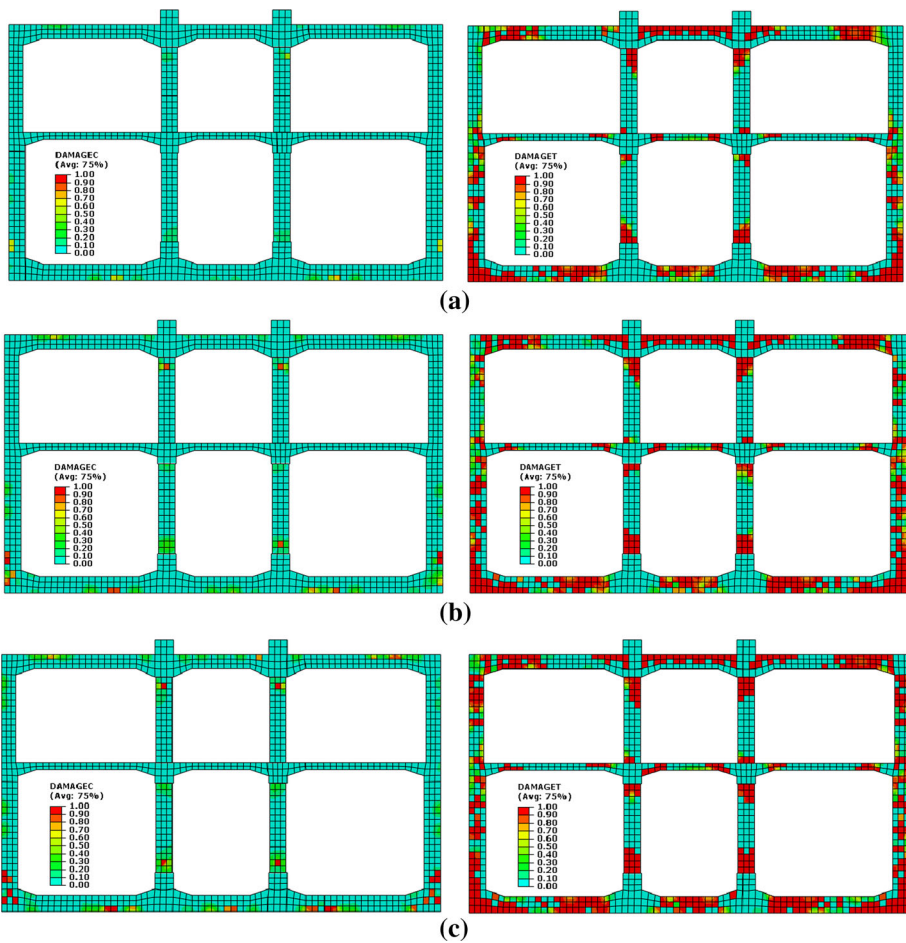


Fig. 26 Damage distributed contour diagram of the subway station in Kobe ground motion. **a** PGA = 0.1 g, **b** PGA = 0.2 g, **c** PGA = 0.3 g

0.7 s and between 1.2 and 2 s. However, with the input PGA increasing to 0.3 g, the acceleration responses in the period near 1 s are amplified obviously and causes no obvious peak acceleration response. Figure 25 also shows a similar finding with the input PGA = 0.3 g for the El-Centro motion.

The above analysis also shows that the liquefied or softened soils around the subway station have greater effects on the acceleration response spectra of the subway station during the longer period than the shorter period. For the lateral deformation of the subway station, the response accelerations are magnified mainly from the bottom to the top of the subway station at period from 0.7 to 2 s with the damping ratio of 5 %.

4.4 Damage of the subway station

To evaluate the damage condition of the subway station, Fig. 26 shows the compression and tensile damage of the subway station in the Kobe motion. Generally, the compression damages of subway station are very slight. The intensity of the input motion has no obvious effect on the compression damage. However, the tensile damage of the subway station is very serious, and it also has been found on the large subway station buried in soft soils (Zhuang et al. 2015).

In Fig. 26a, the subway station is damaged seriously even in low intensity motion, especially at the top slab and the bottom slab. Moreover, the serious tensile damage at the two side ends of the top slab penetrates the whole cross-sections, which are also found at the two cross-sections of the bottom slab, the bottom ends of the columns in under floor, and the two ends of the middle slab in the middle span. With the input PGA increasing, the side walls and the columns in the upper floor are also damaged seriously by the tensile stress, especially at the top ends of these components. Generally, all of the ends of the structure components are almost damaged seriously by the tensile stress in strong intensity motion. Compared with the seismic damage of the subway station buried in non-liquefiable soils (Zhuang and Chen 2006), the tensile damage of the subway station built in liquefiable soils is more serious, which should be mainly caused by the large liquefaction-induced deformation.

5 Conclusions

This study comprehensively examined the effect of soil liquefaction on the seismic responses of a large subway station. A revised constitutive model was implanted into the Abaqus software to address the deficiency of commercial FEM software in modelling the dynamic properties of the liquefiable soils. An advanced numerical model was crafted to model the nonlinear static and dynamic coupling interactions between the soil and the underground structure, the liquefied-induced large deformation of the ground, and the nonlinear properties of the concrete. The liquefaction condition of the ground surrounding the subway station, the seismic deformation and floating behavior of the subway station, and the acceleration response of the subway station were analyzed by using the developed FEM model. The following concluding remarks and recommendations can be made:

1. A revised constitutive model implanted into the Abaqus software can simulate the dilation of the saturated sands during a loading phase and the liquefied-induced large deformation in the vicinity of phase transformation from a contractive response to a dilative response.

2. A large subway station significantly affects the liquefaction behavior of its nearby soils which are more likely to be liquefied than soils that are further away. In addition, the main rising stage of the pore pressure slightly lags behind the strong motion duration of the input ground motions.
3. When the soils surrounding the subway station are liquefied, the subway station severely floats upward. Then, the liquefied soils flow from the side to the bottom of the subway station. Based on this finding, an engineering measure should be installed to block the flow path of the liquefied soils to reduce subway station floating.
4. The floating of the subway station completely lags behind the main vibration ranges of the input ground motions and the main rising stage of the pore pressure, which will only stop when the vibration amplitude of the input ground motion weakens to very low values. Moreover, the subway station inclines slightly in the vertical direction, which should be further studied in detail.
5. As the input PGA increases, the soil liquefaction and soil softening have greater effect on the acceleration response spectra of the subway station in the longer periods than in the shorter periods. The liquefied soils around the subway station could weaken the seismic responses of the subway station. As observed in previous earthquakes, a deep softening soil layer can isolate the seismic response of a large underground structure.
6. For larger underground structures, the surrounding liquefiable soils under the suggested depth of 20 m in many related codes of China may be liquefied under the influence of the subway station floating, which should be considered in the seismic liquefaction estimation of the site for large underground structures.
7. The tensile damage of the subway station built in liquefiable soils is more serious than the same station built in the non-liquefiable soils, of which the distribution is also obviously different as it is governed by the up-lifting deformation pattern of the subway station in the liquefiable soils.

Acknowledgments This research work was funded by research projects from the National Natural Science Foundation of China (Grant No. 51278246) and Natural Science Foundation of Jiangsu Province (CN) (Grant No. BK2012477). The support is gratefully acknowledged. All statements, results, and conclusions are those of the authors and do not necessarily reflect the views of the NSFC.

References

- Azadi M, Hosseini SMM (2010) Analyses of the effect of seismic behavior of shallow tunnels in liquefiable grounds. *Tunn Undergr Space Technol* 25(5):543–552
- Chen GX, Zhuang HY, Du XL et al (2007) Analysis on the earthquake response of subway station built in liquefaction soils by large-scale shaking table testing. *Earthq Eng Eng Vib* 27(3):163–170
- Chen GX, Wang ZH, Zuo X et al (2013) Shaking table test on the seismic failure characteristics of a subway station structure on liquefiable ground. *Earthq Eng Struct Dyn* 42(10):1489–1507
- Chen GX, Chen S, Qi CZ et al (2015) Shaking table test on a three-arch type subway station structure in a liquefiable soil. *Bull Earthq Eng* 13(6):1675–1701
- Chian SC, Madabhushi SPG (2012) Effect of buried depth and diameter on uplift of underground structures in liquefied soils. *Soil Dyn Earthq Eng* 41:181–190
- Chian SC, Tokimatsu K, Madabhushi SPG (2014) Soil liquefaction-induced uplift of underground structures: physical and numerical modeling. *J Geotech Geoenviron Eng* 140(10):31–40
- Chou H, Yang C, Hsieh B, Chang S (2001) A study of liquefaction related damages on shield tunnels. *Tunn Undergr Space Technol* 16(1):185–193
- Chou JC, Kutter BL, Travasarou T, Chacko JM (2010) Centrifuge modeling of seismically induced uplift for the BART transbay tube. *J Geotech Geoenviron Eng* 137(8):754–765
- Drucker DC, Prager W (1952) Soil mechanics and plastic analysis or limit design. *Q Appl Math* 10:157–175

- Hashash Y, Hook J, Schmidt B, Yao J (2001) Seismic design and analysis of underground structure. *Tunn Undergr Space Technol* 16(4):247–293
- Iida H, Hiroto T, Yoshida N, Iwafuji M (1996) Damage to Daikai subway station. *Soils and Foundations, Special Issue on Geotechnical Aspects of the January 17 1995 Hyogoken-Nambu Earthquake*, Japanese Geotechnical Society, 36:283–300
- Iwatate T, Kobayashi Y, Kusu H et al (2000) Investigation and shaking table tests of subway structures of the Hyogoken-Nambu earthquake. In: *The 14th world conference on earthquake engineering*, Beijing, China, Paper No. 1043
- Jeeho L, Fenves GL (1998) Plastic-damage model for cyclic loading of concrete structures. *J Eng Mech* 124(8):892–900
- Liao ZH (2013) *Theories of wave motion for engineering* [M]. Published by Science Press of China
- Liu H, Song E (2006) Working mechanism of cutoff walls in reducing uplift of large underground structures induced by soil liquefaction. *Comput Geotech* 33(4):209–221
- Pyke RM (1979) Nonlinear soil models for irregular cyclic loadings. *J Geotech Geoenviron Eng ASCE* 105(GT6):715–726
- Trifunac MD (2003) Nonlinear soil response as a natural passive isolation mechanism. Paper II. The 1933, Long Beach, California earthquake. *Soil Dyn Earthq Eng* 23(7):549–562
- Unutmaz B (2014) 3D liquefaction assessment of soils surrounding circular tunnels. *Tunn Undergr Space Technol* 40:85–94
- Yang Z (2000) Numerical modeling of earthquake site response including dilatation and liquefaction. PhD Dissertation, Department of Civil Engineering and Engineering Mechanics, Columbia University, New York
- Yang Z, Elgamal A, Parra E (2003) Computational model for cyclic mobility and associated shear deformation. *J Geotech Geoenviron Eng* 129(12):1119–1127
- Zhuang HY, Chen GX (2006) A viscous-plastic model for soft soil under cyclic loadings. *Geotechnical Special Publication of ASCE, Soil and Rock Behavior and Modeling*. In: *Proceedings of the GeoShanghai Conference*, 150:343–350
- Zhuang H, Chen G (2011) Constitutive model for large liquefaction deformation of sand and its implementation in ABAQUS software. *Chin J World Earthq Eng* 27(2):45–50
- Zhuang HY, Cheng SG, Chen GX (2008a) Numerical emulation and analysis on the earthquake damages of Dakai subway station caused by the Kobe earthquake. *Chin J Rock Soil Mech* 29(1):245–250
- Zhuang H, Chen G, Wang X (2008) Study on the earthquake response of subway station built in soft sites with different thickness of soft soil layers. In: *The 14th world conference on earthquake engineering*, October 12–17, 2008, Beijing, China
- Zhuang H, Huang C, Zuo Y (2012) Sensitivity analysis of model parameters for predicting liquefied large deformation of sand. *Chin J Rock Soil Mech* 33(1):280–286
- Zhuang H, Hu Z, Chen G (2015) Numerical modeling on the seismic responses of a large underground structure in soft ground. *J Vibroeng* 17(2):802–815